Effect of halogenated spacer cation on structural symmetry breaking in 2D halide double perovskites

Puneet Siwach,[1] Poonam Sikarwar,[1] Shubham Ajaykumar Rajput,[1] Sudhadevi Antharjanam,[2] Aravind Kumar Chandiran[13*]

[1]Department of Chemical Engineering, Indian Institute of Technology Madras, Adyar, Chennai, Tamil Nadu 600036, India

[2]Sophisticated Analytical Instrument Facility, Indian Institute of Technology Madras, Adyar, Chennai, Tamil Nadu 600036, India

[3]Centre for Photo- and Electro-Chemical Energy Sciences (C-PEC), Indian Institute of Technology Madras, Adyar, Chennai, Tamil Nadu 600036, India

Electronic Supplementary Information

Experimental Methods

Chemicals Used. 3-bromopropylamine hydrobromide ($BrC_3H_8N.HBr$, 98%, Sigma Aldrich, 3-BPA), 3-chloropropylamine hydrochloride ($ClC_3H_8N.HCl$, 98%, Alfa Aesar, 3-CPA), bismuth bromide ($BiBr_3$, 99% Alfa Aesar), silver bromide (AgBr, 99.5%, Alfa Aesar), silver oxide (Ag_2O, 99%, Sigma Aldrich), hydrobromic acid (HBr, Spectrochem) and diethyl ether ($C_4H_{10}O$, Rankem) were procured for synthesis and all these chemicals were used without any further purification.

Synthesis of layered halide perovskites. The stoichiometric mixture of 3-bromopropylamine hydrobromide (2 mmol), silver bromide (0.5 mmol) and bismuth bromide (0.5 mmol) were dissolved in 2 ml of HBr under heating and continuous stirring at 100 °C for 45 min to achieve the clear solution. This solution was then slowly cooled down to room temperature to obtain the millimetre sized yellow crystals of $(3\text{-}BPA)_4AgBiBr_8$ (BPA). The same procedure was used for $Cl_{0.97}Br_{3.03}PA_4AgBiBr_8$(CPA) crystal synthesis with 3-chloropropylamine hydrochloride (2 mmol), silver oxide (0.25 mmol) and bismuth bromide (0.5mmol) precursors. To obtain the powder materials, the products were synthesized with quick cooling which were filtered followed by washing with diethyl ether, then dried it in the hot air oven at 70°C for 24 hours and finally grounded with mortar and pestle.

Structural Characterization. Single crystals X-ray diffraction (SC-XRD) analysis was carried out at 220 K on Bruker D8 VENTURE single-crystal X-ray diffractometer equipped with Mo Kα X-ray radiation (λ = 0.71073 Å) source and PHOTON II detector to collect the phase and crystal structure data of BPA and CPA materials. The collected data was resolved and refined using WINGX-SHELX software and then CIF check was carried out on IUCR. The crystal structures were drawn using the CIF files on VESTA, version-3 software for visualisation and finding the bond lengths and bond angles to calculate the degree of distortion (λ, σ^2). Powder XRD (PXRD) measurements were performed on Rigaku X-ray powder diffractometer having Cu-Kα source with 1.5406 Å wavelength at a step size of 0.01° over the 2θ range of 5-40 degrees. JASCO 6600FV spectrometer fitted with ATR setup was

used for FTIR measurements operated under ambient and vacuum for IR and far-IR region respectively, from 6000 cm^{-1} to 50 cm^{-1}. Raman spectra was collected from Horiba - Yvon (HR-800UV) micro Raman spectrometer with 632 nm laser excitation source.

Thermal stability measurements. Differential scanning calorimetric (DSC) measurements were performed on NETZSCH DSC 204F1 Phoenix between -100 °C and 120 °C with 10 °C per minute heating rate in nitrogen atmosphere. The reference used in DSC study was Al crucible with pierced lid. Thermal Gravimetric Analysis (TGA) of CPA and BPA was measured under inert (N_2) atmosphere from room temperature to 900 °C on SDT Q600 T.A. instruments and with a temperature step size of ±10.0 °C/min.

Optical measurements. The UV-Vis absorption spectra of the powdered materials was obtained on Shimadzu 2600 spectrophotometer equipped with barium sulphate-coated integrating sphere. Room temperature steady state emission (PL) spectra was recorded using Horiba Fluorolog Spectrofluorometer (Flurolog-3) containing a 450 W xenon arc lamp. To avoid the second order diffraction in the emission, suitable long-pass cut-off filters were used at the entry port of the emission monochromator. Lifetime measurements were also conducted on the same equipment with 401 nm nanoLED laser diode that provide pulse duration less than 200 ps. The obtained data was fitted by Horiba Datastation software. The photoluminescence quantum yield (PLQY) was determined using the same machine with integrating sphere (K-Sphere, Horiba). The colour coordinates are specified by Commission International de L' Eclairage (CIE-1931) chromaticity coordinates and are calculated on a chromaticity diagram. These colour coordinates are calculated from the PL emission spectra on Horiba Fluorolog Spectrofluorometer (Flurolog-3).

Polarization-Electric filed (P-E) hysteresis studies: The P-E hysteresis loop was carried out on the BPA and CPA crystals using the aixACCT Systems GmbH (Aachen Germany) TF Analyser 3000 fitted with 150 V inbuilt amplifier and externally attached with Trek 1 KV/10 KV amplifier connected to the Thin Film Sample Holder (TFSH) unit with HV-extension. Samples were prepared on the microscopic slides using the single crystals of BPA and CPA and contacts were made using the conductive silver paste. The tungsten wire probes (American Probe & Technologies, Inc.) with a radius of 1 µm were used in the TFSH Unit and were mounted with utmost care to make contacts with the single crystals without breaking them. The optical images of the different single crystal configurations were captured using a USB microscope camera (The Imaging Source Europe GmbH - Germany) attached to the TFSH Unit. The loop was measured using the triangular waveform for two different configurations of single crystals including top-bottom and side configuration.

AFM-PFM studies: The atomic force microscopy (AFM) studies were carried out on the BPA and CPA crystals using the Oxford Instruments (Asylum Research, Santa Barbara, CA) MFP-3D Origin+ AFM with the resonant enhanced piezoelectric force microscope (PFM) mode to obtain the morphological images of the single crystals for analysing the piezoelectric behaviour. All AFM and PFM measurements were captured using Pt/Ir coated cantilevers with a spring constant of 1.7 N/m and a resonance frequency of ~61 kHz.

Results & Discussion: Optical Properties of BPA and CPA

The UV-Vis spectra shown in Figure S8 has absorption onset at ~505 nm (2.45 eV) for CPA and BPA. It has already been reported that PA has a bandgap of 2.39-2.41 eV which is comparable to CPA and BPA, however, its 3D analogue, $Cs_2AgBiBr_6$ has a lower bandgap of 2.2 eV.[1] The valence band maximum (VBM) in $Cs_2AgBiBr_6$ is formed by Ag-*4d*, Br-*4p* and Bi-*6s* orbitals and conduction band minimum (CBM) has Ag-*5s*, Bi-*6p* and Br-*4p* orbitals.[2–4] These results are indicating no direct effect of different organic moieties however, the variation in bandgap in layered structures might arise from the inter- and intra-octahedral distortion caused by the difference in orbital overlap between Ag/Bi-Br.[5] Although the distortion is different for all the layered structures, the bandgap remained the same. This shows that beyond a certain critical distortion (λ, σ^2), the optical bandgap doesn't get affected significantly. Both CPA and BPA show broad photoluminescence emission spectra from 380 to 550 nm (**Figure 4(a)**, Figure S9-S10) with former showing relatively higher emission. The PLQY of CPA is 0.36 and it is slightly higher than BPA which is 0.33. Their CIE coordinates are in the blue region (Table S4, Figure S11). The photoluminescence decay measurement also showed higher excited-state lifetime of several *ns* for CPA, whereas for BPA the decay overlaps with the instrument response indicating *sub-ns* lifetime. There is no clear trend of distortion to the lifetime in these materials.[6] Further work on theoretical simulations shall help understanding these properties better.

Table S1 Crystal data and structure refinement for BPA and CPA.

Compound	Br$_4$PA$_4$AgBiBr$_8$ (BPA)	Cl$_{0.97}$Br$_{3.03}$PA$_4$AgBiBr$_8$ (CPA)
Empirical formula	C12 H36 Ag Bi Br12 N4	C12 H36 Ag Bi Br11.03 Cl0.97 N4
Formula weight (g.mol^{-1})	1512.22	1469.09
Temperature (K)	220(2)	220(2)
Wavelength (Å)	0.71073	0.71073
Crystal system	Monoclinic	Monoclinic
Space group	Pc	Pc
Unit cell dimensions (Å)	a = 8.8204(5) Å; α = 90° b = 7.9482(6) Å; β = 91.046(2)° c = 25.6987(17) Å; γ = 90°	a = 8.7776(12) Å; α= 90° b = 7.9372(10) Å; β= 90.543(5)° c = 25.632(4) Å; γ = 90°.
Volume (Å^3)	1801.3(2)	1785.7(4)
Z value	2	2
Density (calculated) (Mg/m^3)	2.788	2.732
Absorption coefficient (mm^{-1})	18.741	17.893
F(000)	1372	1337
Crystal size (mm^3)	0.100 x 0.100 x 0.050	0.150 x 0.100 x 0.100
Theta range for data collection	2.563 to 24.997°	2.384 to 24.996°
Index ranges	-10<=h<=10, -9<=k<=9, -30<=l<=30	-10<=h<=10, -9<=k<=9, -30<=l<=30
Reflections collected	38135	38684
Independent reflections	38135[#]	6273 [R(int) = 0.0667]
Completeness to theta = 24.997°	99.7 %	99.9 %
Absorption correction	Semi-empirical from equivalents	Semi-empirical from equivalents
Max. and min. transmission	0.52 and 0.36	0.6471 and 0.3411
Refinement method	Full-matrix least-squares on F^2	Full-matrix least-squares on F^2
Data / restraints / parameters	38135 / 578 / 295	6273 / 542 / 332
Goodness-of-fit on F^2	1.082	1.090
Final R indices [I>2sigma(I)]	R1 = 0.0736, wR2 = 0.1853	R1 = 0.0787, wR2 = 0.2067
R indices (all data)	R1 = 0.0873, wR2 = 0.1966	R1 = 0.0885, wR2 = 0.2195
Extinction coefficient	n/a	n/a
Largest diff. peak and hole (eÅ^3)	3.438 and -2.468	2.537 and -2.343

[#] The crystal lattice of Br$_4$PA$_4$AgBiBr$_8$ is twinned and equivalent reflections are not merged. Hence the R(int) values couldn't be calculated by the program.

Table S2 Bond length distortion and bond angle variance values for PA, BPA and CPA. In BPA and CPA, the halogens and central metal atoms are located at two neighbouring sites, sharing the occupancy. This table gives the data where the elements are at highest occupancy.

Material	Bond Length Distortion (λ)		Bond Angle Variance (σ^2)	
	Bi octahedron	Ag octahedron	Bi octahedron	Ag octahedron
PA	$0.25*10^{-4}$	$3*10^{-3}$	1.67	13
BPA	$3.3*10^{-4}$	$11*10^{-3}$	37.3	86.9
CPA	$5*10^{-4}$	$8.6*10^{-3}$	57.2	41

Table S3 Bond length distortion and bond angle variance values for PA, BPA and CPA. In BPA and CPA, the halogens and central metal atoms are located at two neighbouring sites, sharing the occupancy. This table gives the data where the elements are at lowest occupancy.

Material	Bond Length Distortion (λ)		Bond Angle Variance (σ^2)	
	Bi octahedron	Ag octahedron	Bi octahedron	Ag octahedron
PA	0	0	0	0
BPA	$4*10^{-4}$	$11*10^{-3}$	16.3	73.8
CPA	$6.4*10^{-5}$	$20*10^{-3}$	45.2	209

Table S4 Quantum yield value and colour coordinates of BPA and CPA material.

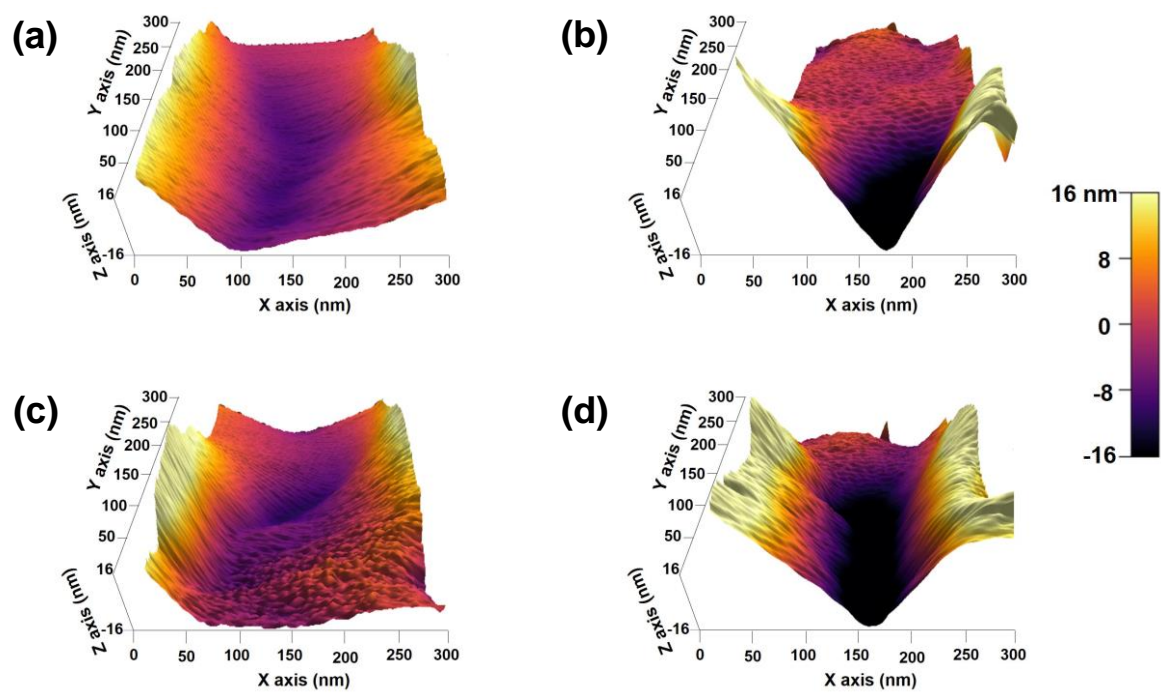| Material	PLQY	Colour Coordinates	
		x	y
BPA	0.33	0.22	0.196
CPA	0.36	0.22	0.196

Figure S1. PFM topographical imaging of BPA ((a) Tip 1 V and (c) Tip 5 V), and CPA ((b) Tip 1 V and (d) Tip 5 V).
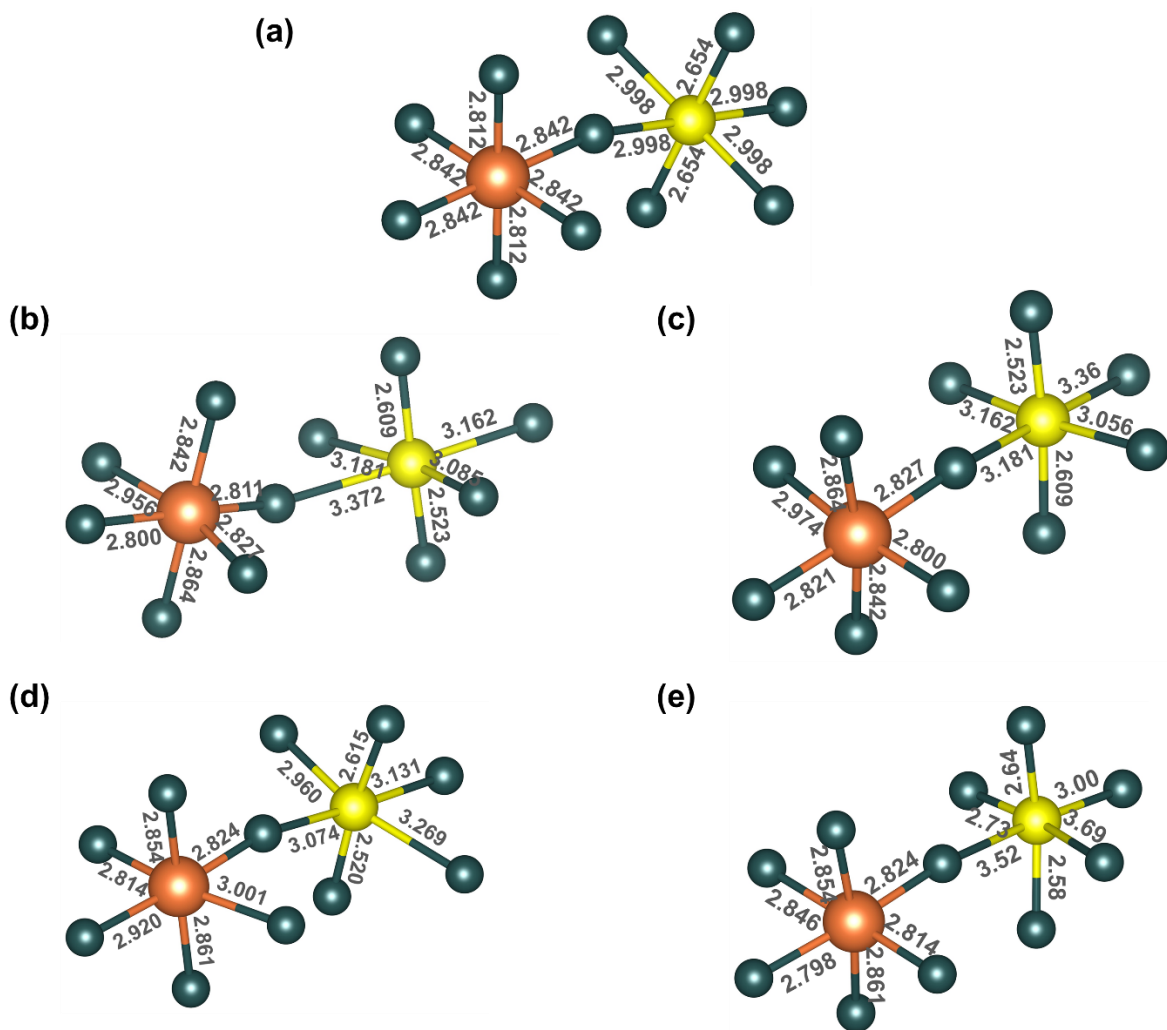
Figure S2. (a), (b) and (d) represents octahedral arrangement of PA, BPA and CPA respectively for elements with maximum occupancy. (c) and (e) shows the octahedral arrangement of BPA and CPA respectively for elements with lower occupancy.
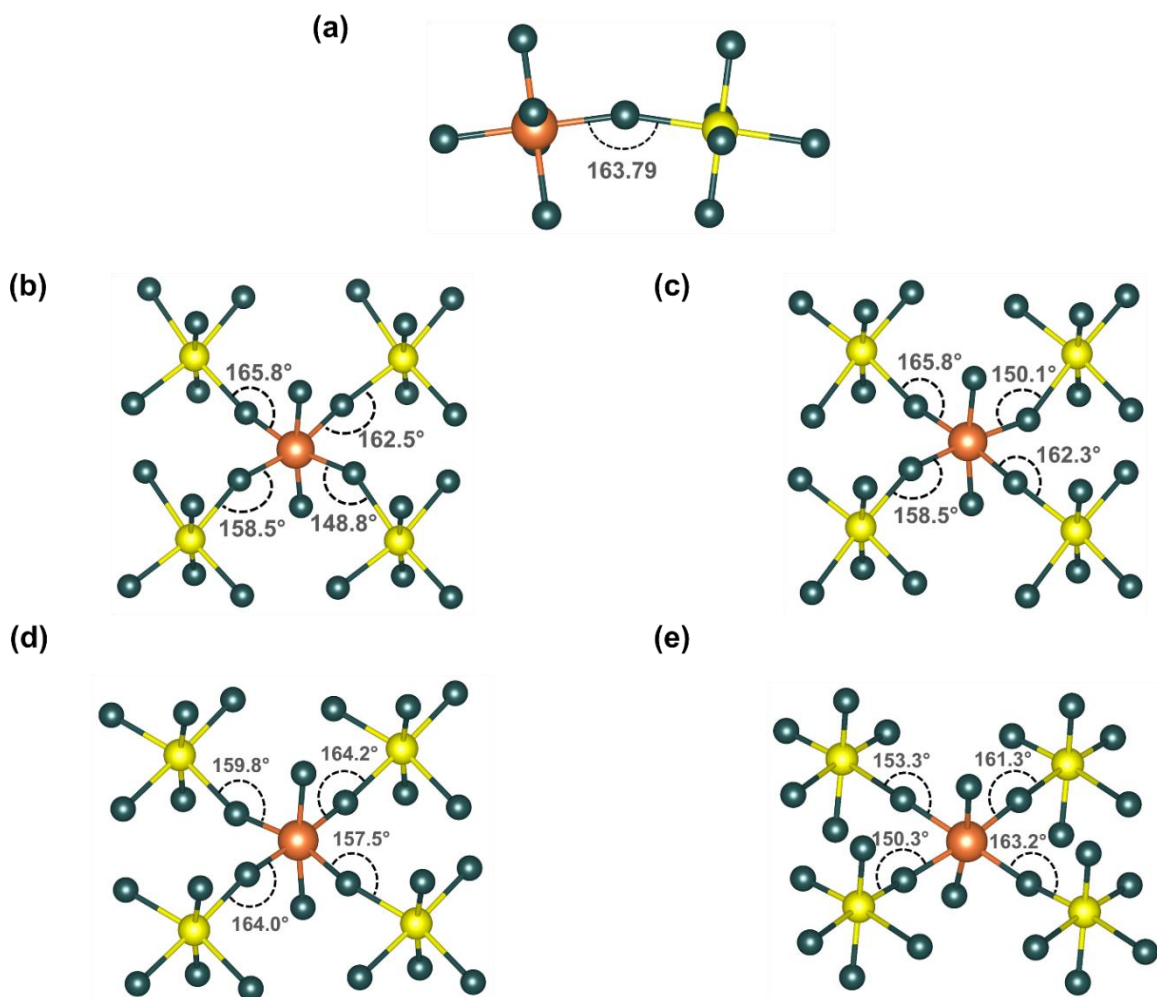
Figure S3. (a), (b) and (d) represents single crystal X-ray structures of PA, BPA and CPA respectively with inter-octahedral distortion for elements with maximum occupancy. (c) and (e) shows the single crystal X-ray of BPA and CPA, respectively with inter-octahedral twist for elements with lower occupancy.
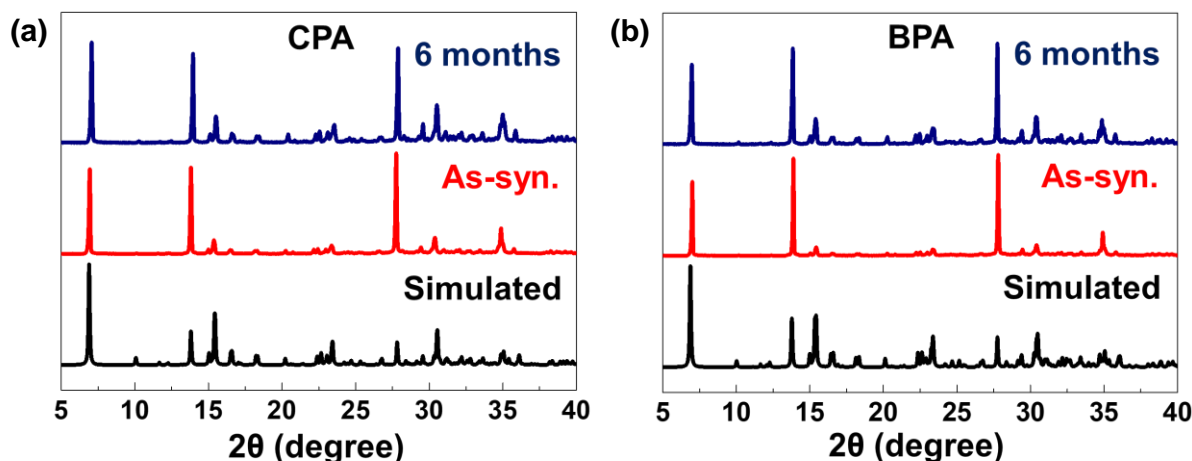
Figure S4. (a), (b) Power XRD comparison between simulated, as-synthesized and after 6 months' stability of CPA and BPA compounds. The powders of these materials were synthesized by fast cooling the reactant solution and their properties were investigated. The patterns match with the simulated XRD generated using CIF data and it indicates the phase purity of powder materials.
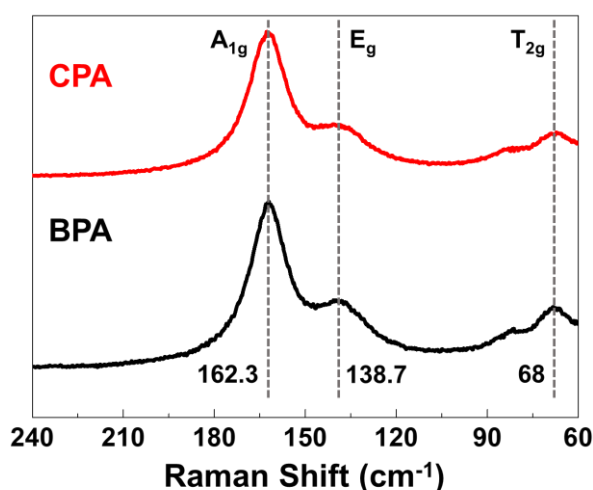
Figure S5. Raman spectra of CPA and BPA powder samples with dotted lines represent the peak points. Three distinct peaks were observed: A_{1g} at 162.3 cm^{-1}, E_g at 138.7 cm^{-1} and T_{2g} at 68 cm^{-1} for both CPA and BPA, although shift in peaks were observed for A_{1g}. The latter is a result of softening of phonon modes due to break in octahedral connectivity in the third dimension.
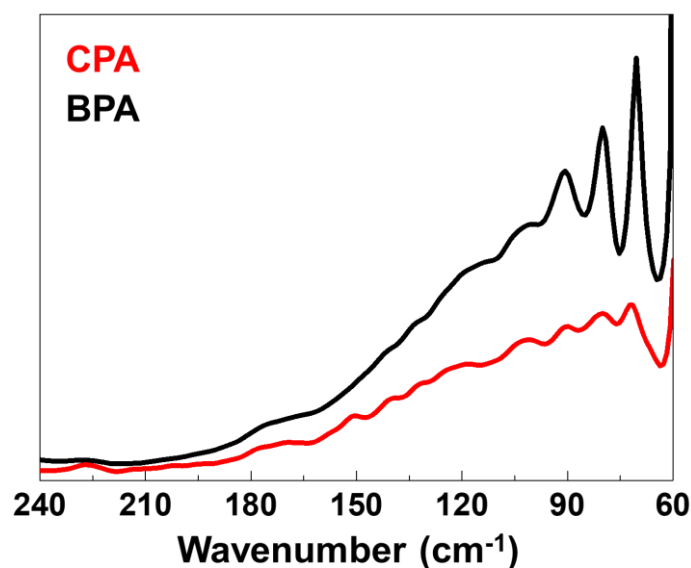
Figure S6. FTIR spectra of CPA and BPA materials in far-IR region. All results presented here are taken at room temperature. For a typical symmetric octahedra, there should be two IR-active vibrational modes (bending (b) and stretching(s)) and any break in symmetry splits the two peaks further. In our previous work on $Cs_2AgBiCl_6$, we have shown two distinct peaks for every octahedra, one set at higher wavenumbers (158 cm^{-1}(s), 103 cm^{-1}(b)) and another set at lower wavenumbers (70 cm^{-1}(s), 56 cm^{-1}(b)) for $[BiCl_6]^{3-}$ and $[AgCl_6]^{5-}$ respectively.[7] We have also shown that these peaks split into multiple peaks as the symmetry of the octahedron reduces from O_h to C_{4h} and further down. In CPA and BPA, the octahedra doesn't possess any rotational symmetry, making them completely asymmetric, leading to multiple peaks in FTIR spectra. This result confirms the presence of distortion in powder materials.
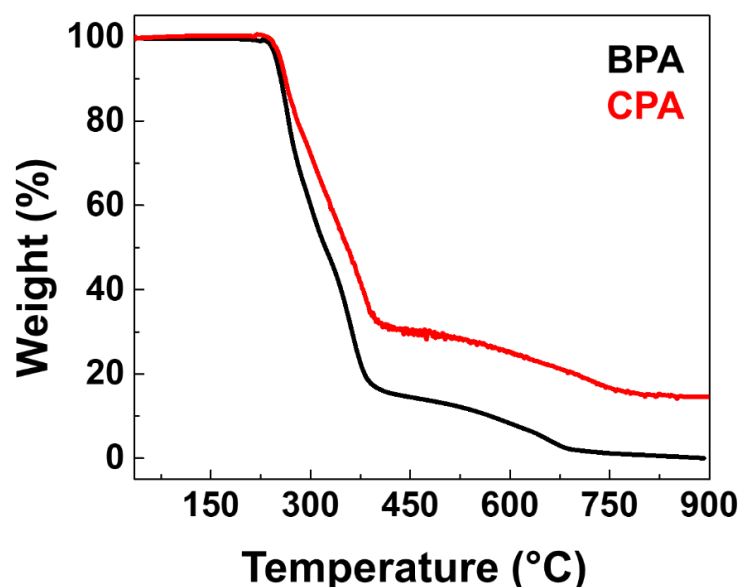

Figure S7. Thermal Gravimetric Analysis (TGA) of CPA and BPA materials. The TGA data shows that both these materials remain stable approximately until 240 °C (99% of weight retention), followed by steep loss in weight possibly due to degradation of organic cations.
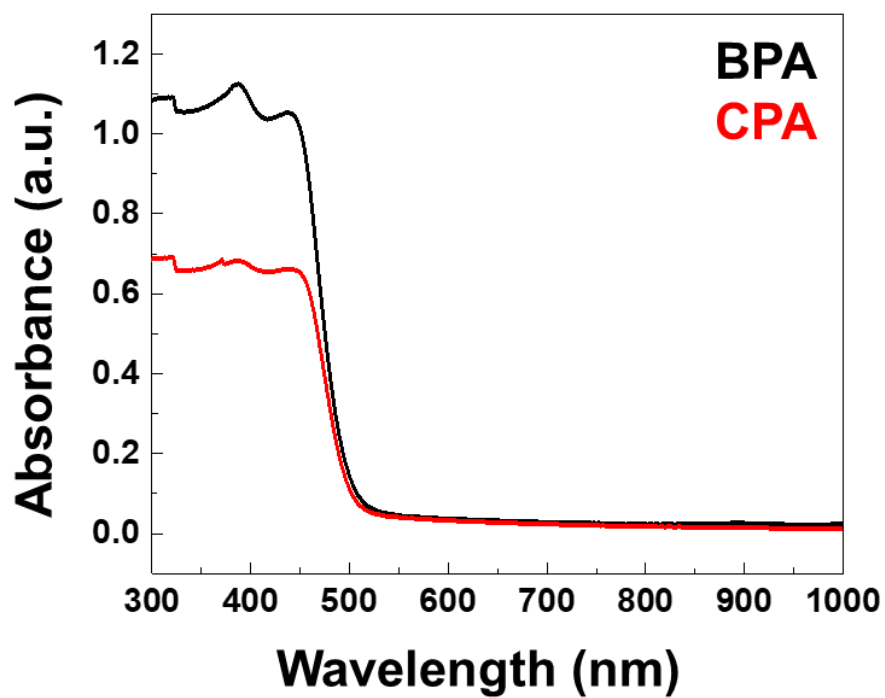
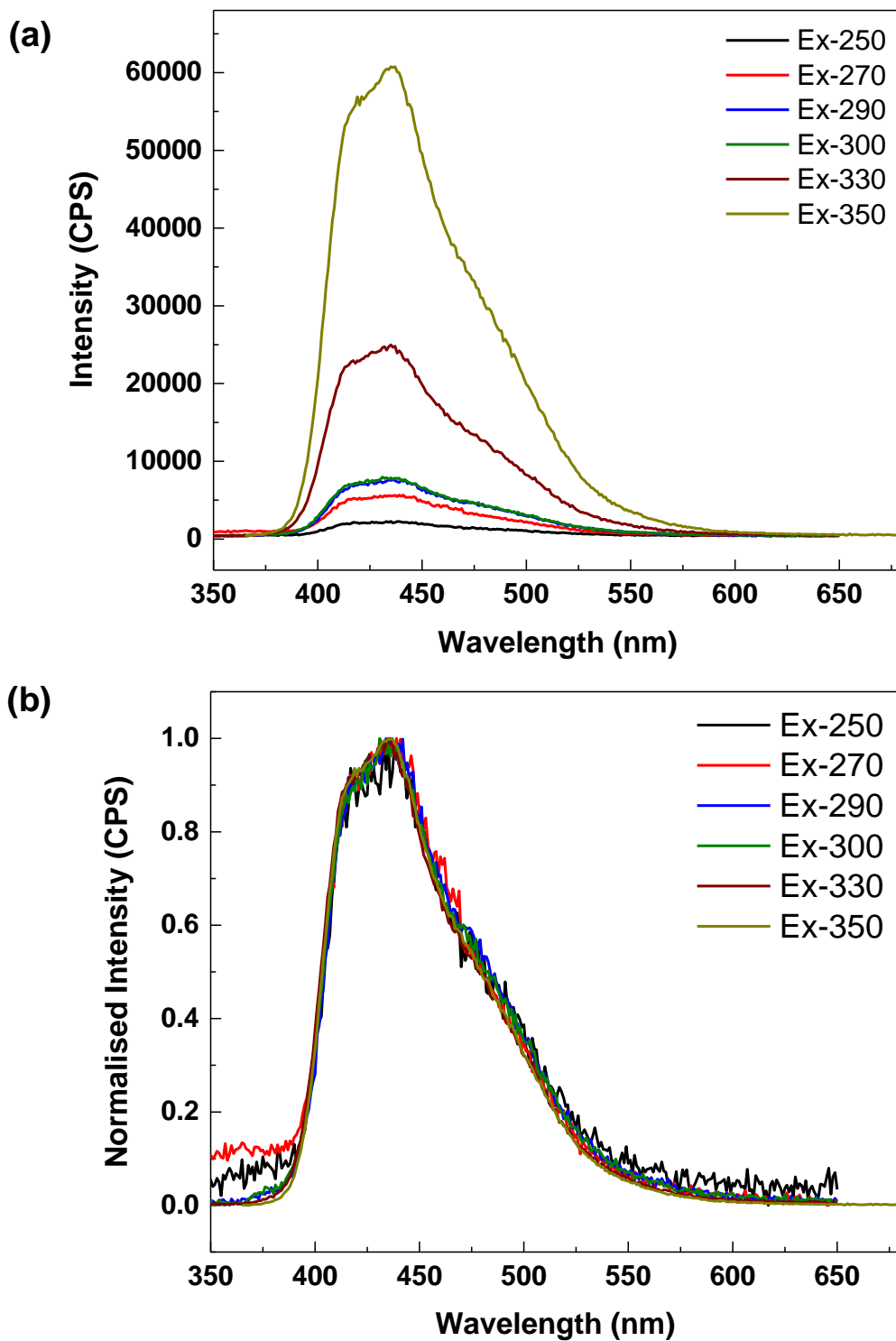**Figure S8.** Absorption spectra of CPA and BPA materials.

Figure S9. Photoluminescence emission spectra of CPA (a) at different excitation wavelengths and (b) its normalised spectra. The excitation wavelengths are given in the figure legends.
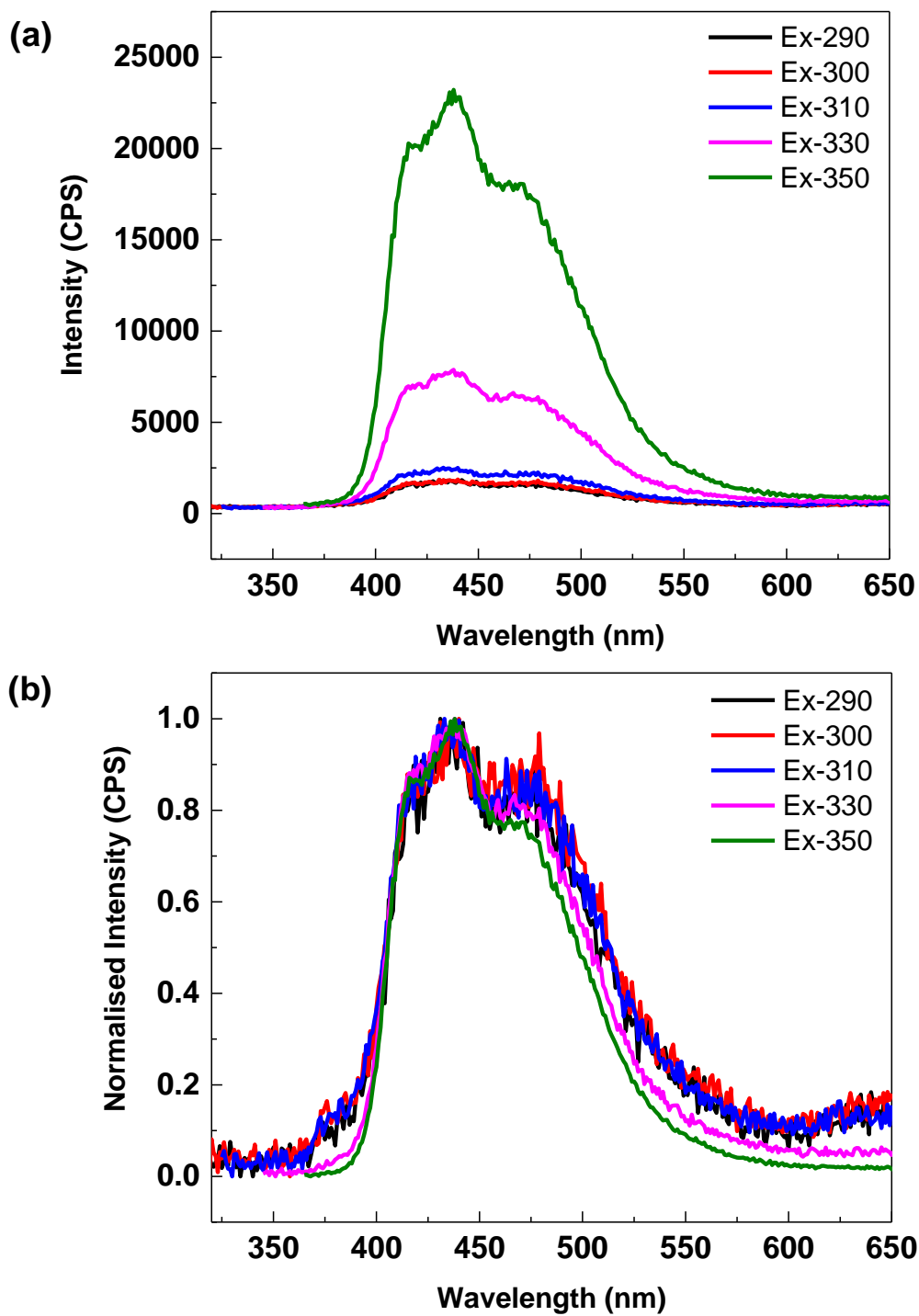
Figure S10. Photoluminescence emission spectra of BPA (a) at different excitation wavelengths and (b) its normalised spectra. The excitation wavelengths are given in the figure legends.
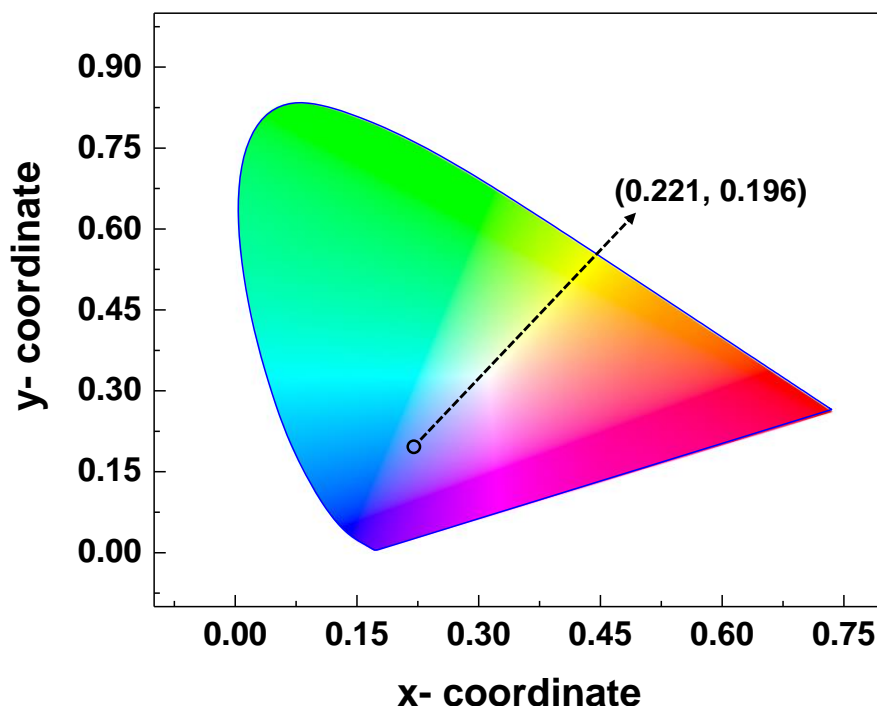
CIE 1931

Figure S11. CIE (Commission Internationale de l'éclairage) colour coordinates x and y for CPA and BPA showing emission in blue region.

References

1   L. Mao, S. M. L. Teicher, C. C. Stoumpos, R. M. Kennard, R. A. Decrescent, G. Wu, J. A. Schuller, M. L. Chabinyc, A. K. Cheetham and R. Seshadri, *J. Am. Chem. Soc.*, 2019, **141**, 19099–19109.

2   M. R. Filip, S. Hillman, A. A. Haghighirad, H. J. Snaith and F. Giustino, *J. Phys. Chem. Lett.*, 2016, **7**, 2579–2585.

3   A. H. Slavney, L. Leppert, D. Bartesaghi, A. Gold-Parker, M. F. Toney, T. J. Savenije, J. B. Neaton and H. I. Karunadasa, *J. Am. Chem. Soc.*, 2017, **139**, 5015–5018.

4   E. T. McClure, M. R. Ball, W. Windl and P. M. Woodward, *Chem. Mater.*, 2016, **28**, 1348–1354.

5   B. Luo, Y. Guo, Y. Xiao, X. Lian, T. Tan, D. Liang, X. Li and X. Huang, *J. Phys. Chem. Lett.*, 2019, **10**, 5271–5276.

6   S. Raugei, M. L. Helm, S. Hammes-Schiffer, A. M. Appel, M. O'Hagan, E. S. Wiedner and R. M. Bullock, *Inorg. Chem.*, 2016, **55**, 445–460.

7   T. Appadurai, R. Kashikar, P. Sikarwar, S. Antharjanam, B. R. K. Nanda and A. K. Chandiran, *Commun. Mater.*, 2021, **2**, 68.